PROTEINS: Structure, Function, and Bioinformatics 66:538–546 (2007)

Serendipitous Discovery of Novel Bacterial Methionine Aminopeptidase Inhibitors

Artem G. Evdokimov,[1]* Matthew Pokross,[1] Richard L. Walter,[2] Marlene Mekel,[2] Bobby L. Barnett,[1] Jack Amburgey,[3] William L. Seibel,[1] Shari J. Soper,[3] Jane F. Djung,[3] Neil Fairweather,[3] Conrad Diven,[1] Vinit Rastogi,[1] Leo Grinius,[3] Charles Klanke,[3] Richard Siehnel,[3] Tracy Twinem,[4] Ryan Andrews,[4] and Alan Curnow[2]

[1]*Structural Biology Core Facility, The Procter & Gamble Pharmaceuticals, Mason, Ohio*
[2]*Central Research Division, Miami Valley Laboratories, The Procter & Gamble Company, Cincinnati, Ohio*
[3]*Anti-Infective Focus Area, The Procter & Gamble Pharmaceuticals, Mason, Ohio*
[4]*Protein Engineering Core Facility, The Procter & Gamble Pharmaceuticals, Mason, Ohio*

ABSTRACT **In this article we describe the application of structural biology methods to the discovery of novel potent inhibitors of methionine aminopeptidases. These enzymes are employed by the cells to cleave the N-terminal methionine from nascent peptides and proteins. As this is one of the critical steps in protein maturation, it is very likely that inhibitors of these enzymes may prove useful as novel antibacterial agents. Involvement of crystallography at the very early stages of the inhibitor design process resulted in serendipitous discovery of a new inhibitor class, the pyrazole-diamines. Atomic-resolution structures of several inhibitors bound to the enzyme illuminate a new mode of inhibitor binding. Proteins 2007;66:538–546.** © 2006 Wiley-Liss, Inc.

Key words: structure-based; drug design; virtual screening; antibacterial; methionine aminopeptidase

INTRODUCTION

Methionine aminopeptidases (MAPs) facilitate the removal of the N-terminal methionine from nascent polypeptides.[1] Bacterial MAPs are targets for antimicrobial therapy,[1] whereas the structurally similar human MAP-2 is a target for anticancer agents[2,3]; therefore, discovery of new inhibitors offers hope for treatment of microbial infections as well as cancer.

Discovery of novel pharmaceutically interesting molecules remains an arduous, expensive, and uncertain process.[4] No single method has yet emerged as the means to provide the ultimate solution to drug discovery problems, therefore diverse methodologies ranging from high-throughput screening to modeling and structure-based *de novo* drug design are employed, often in parallel, to maximize the probability of success. The structure-based methods of drug discovery are typically employed in the later stages of the design process, usually when the lead candidates have already been identified and verified. We believe, however, that involvement of structural biology at the very early stages of drug discovery process can help eliminate false leads as well as provide structural data, inaccessible via any other methods. Herein we describe the serendipitous discovery of pyrazole-diamines (PDAs)—a novel class of MAP inhibitors that chelate both active site cobalt ions via a single heterocycle. With the aid of atomic-resolution crystal structures, enzyme assay data, and macromolecular NMR we compare the PDAs with the inhibitors based on a previously described scaffold[2] and offer routes for development of compounds with valuable pharmacological properties.

MATERIALS AND METHODS

Chemistry

PDAs and related entities used in this study were obtained directly from a subset of our compound repository, which had been procured from multiple chemical vendors. Their purity and chemical identity were verified via crystallography, MS and 1D NMR (data not shown). Chemical synthesis of amino alcohols (AA) used in this article will be described elsewhere.

Protein Expression, Purification, Characterization, and Crystallization

Fll-length untagged *Ec*MAP was expressed in *E. coli* from a pET28a vector backbone (Novagen) and purified essentially as described earlier.[5] Uniformly ^{15}N-labeled enzyme was obtained in the same fashion using *E. coli* cells grown on M9 medium using $^{15}NH_4Cl$ as sole nitrogen source. Purified enzyme was concentrated to 12 mg/mL in solution containing 150 m*M* NaCl, 10 m*M* methionine, 0.5 m*M* $CoCl_2$, 0.02% β-octyl glucoside, and 25 m*M* Tris-HCl pH 7.4. This solution can be snap-frozen in liquid nitrogen and stored indefinitely at -80°C without loss of activity. Enzyme activity of *Ec*MAP was tested using the previously published assay[6] and was found to be in good correspondence with previously published values. The enzyme was also characterized by mass spectrometry, and as expected, complete loss of the initiator methionine

*Correspondence to: Artem G. Evdokimov, P & G Pharmaceuticals, 8700 Mason-Montgomery road, Mason, OH, 45040.
E-mail: artem@xtals.org

Received 30 March 2006; Revised 23 July 2006; Accepted 8 August 2006

Published online 21 November 2006 in Wiley InterScience (www.interscience.wiley.com). DOI: 10.1002/prot.21207

was observed, resulting in apparent *Ec*MAP m.w. of 29,199.7 Da (theoretical m.w. without initiator methionine is 29,199.86 Da). Dynamic light scattering showed narrow unimodal distribution of particle sizes, in good correlation with the protein being a monomer in solution.

Use of the published crystallization conditions[7] produced crystals in our hands that diffract to 2.2 Å resolution using our home source. To improve the diffraction quality, we utilized batch crystallization as follows: 100 μL of protein solution (10–12 mg/mL) containing 2–5 m*M* inhibitor were thoroughly mixed with 100 μL of precipitant (25% PEG8000, 100 m*M* Tris-HCl, pH 7.0); the resulting cloudy solution was clarified by centrifugation (14,000*g* for 2 min) and deposited into glass depression plates. Immediately upon setup, the wells were streak-seeded (using a cat whisker dipped into crushed previously grown crystals) and covered with Crystal-Clear™ tape. Within 2–7 days the crystals grew to 0.2 mm in maximum dimension. For cryoprotection the crystals were immersed in Paratone™ oil, all adhering solvent was removed using a microfilament loop and paper wicks, and the crystals were flash-frozen in a stream of nitrogen at 100 K. This procedure allowed us to collect diffraction data up to 1.9–1.4 Å resolution at home and to 1.2–1.0 Å resolution using the IMCA-CAT ID-17 and BM-17 beamlines at the Argonne Advanced Photon Source.

Structure Solution and Refinement

The structures were solved by molecular replacement (AMoRe[8]) using the previously published structure of *Ec*MAP/norleucine phosphonate complex (PDBID: 1C27) as a starting model. After several rounds of manual and automated rebuilding using Quanta™ (Accelrys), O[9], and Coot,[10] the models were initially refined to convergence using SHELXL-97[11] followed by final refinement in Refmac5.[12] Chemically reasonable structures for the charge-neutral forms of ligands were generated using Spartan (Wavefunction) and energy-minimized as described earlier[13] using Gaussian-98.[14] Because of the high resolution of the available data, unrestrained refinement of the metal ion coordination spheres was possible. Water molecules were added using Coot and verified manually. Where warranted by data resolution and quality, we refined the nonhydrogen atoms anisotropically and used the "riding model" for hydrogens. A brief summary of essential data collection and structure refinement parameters is given in Table I.

Enzyme Assays

The inhibitory activity of a compound toward *Ec*MAP was measured by incubating the compound at various concentrations in the presence of the enzyme and the peptide substrate MGMM. After a set period of time, the reactions were quenched with TFA and analyzed by the HPLC method established by Larrabee et al.[6]

Nuclear Magnetic Resonance

^{15}N-H heteronuclear correlation spectra were collected on a Varian-500 instrument using standard pulse programs. Protein concentration was kept at 10 mg/mL in perdeuterated Tris buffer pH 7.5, 100 m*M* NaCl, and 10% D_2O for internal lock standard.

Quantum–Mechanics Calculations

All QM calculations were performed using Gaussian-98[14] set up for density functional theory simulations of small organic molecules, as described earlier.[13] Gaussian-98 jobs were launched on a Linux 64-CPU cluster via Spartan that was also used to analyze the resulting computational models and to plot the electron density distributions.

RESULTS

Our search for MAP inhibitors started with a ~500,000-compound virtual screen using a previously published *Escherichia coli* MAP (*Ec*MAP) structure as the virtual target. Compounds for screening were selected from our chemical repository and vendors' databases. Virtual hit compounds were obtained from the repository or the respective vendor and their *Ec*MAP IC_{50} values were measured. Among the scores of hits was compound **1** (see Fig. 1). Computational modeling of **1** in complex with *Ec*MAP suggested that the ligand was bound to the dicobalt active site via the carboxylic group. The compound inhibited *Ec*MAP with good potency (1.75 μ*M* IC_{50}); however all tested structural analogues of **1** were inactive in the in vitro assay.[6] Fortunately, we were able to cocrystallize the enzyme in complex with **1** and determine the X-ray diffraction structure of the complex at 1.1 Å resolution. Immediately, it became clear that not only the initial model of **1** binding to *Ec*MAP was incorrect but that the chemical structure of the lead compound was not **1** but **2** (Fig. 1). Since compounds **1** and **2** are connectivity isomers of one another, they are practically impossible to distinguish by mass spectrometry or elemental analysis, which are standard techniques for purity control. Likewise, ^{1}H- or ^{13}C-NMR spectra were not very helpful in this case.

Once the true identity of the compound was established, we were able to locate its active structural relatives using substructure and similarity searches. Approximately 50 analogues of **2** were found in our repository. Ten compounds with IC_{50} values in the 20–0.25 μ*M* range were selected for structural studies (Table II). We shall refer to these compounds and their relatives as PDAs because of the importance of that heterocycle for *Ec*MAP inhibition.

Crystallography of *Ec*MAP Complexes

In total, we cocrystallized *Ec*MAP in complex with five PDAs (Table II) and solved X-ray crystal structures of these complexes at resolutions ranging from 1.0 to 2.1 Å. We also solved several structures of *Ec*MAP complexes with four chiral AAs (Table III) that were designed based on a previously published transition-state analogue scaffold.[2,7] In addition, we were able to determine the structure of the *Ec*MAP-methionine complex at 1.0 Å resolution. All these structures were deposited with the Protein Data Bank (RCSB), please refer to Tables II and III for PDBid values.

PROTEINS: Structure, Function, and Bioinformatics DOI 10.1002/prot

TABLE I. Essential Crystallographic Data Collection and Structure Refinement Parameters

Compound	Met	2	3	4[a]	7[a]	12	13[a]	14[a]	15[a]
X-ray source	IMCA	IMCA	IMCA	Home	IMCA	IMCA	IMCA	Home	IMCA
a (Å)	38.75	39.12	39.37	38.78	39.05	39.48	39.13	38.72	38.70
b (Å)	59.47	62.95	63.20	61.46	62.74	63.06	63.29	61.45	62.02
c (Å)	51.20	52.74	52.51	53.90	52.67	52.64	52.51	53.31	53.26
β (°)	111.64	109.01	109.55	107.67	108.85	109.88	109.71	107.08	107.47
Resolution (Å)[b]	1.05 (1.15–1.05)	1.10 (1.25–1.10)	1.00 (1.10–1.0)	2.12 (2.25–2.12)	1.45 (1.55–1.45)	1.28 (1.40–1.28)	1.05 (1.15–1.05)	2.13 (2.25–2.13)	1.8 (1.9–1.8)
Completeness (%)[b]	93.2 (73.2)	99.6 (99.2)	94.0 (88.5)	94.4 (76.5)	96.4 (85.3)	93.0 (79.3)	99.7 (99.4)	99.3 (96.6)	92.9 (92.7)
Redundancy[b]	2.6 (1.5)	2.8 (1.4)	2.1 (1.2)	2.2 (1.4)	2.5 (1.2)	2.0 (1.1)	2.9 (1.6)	2.7 (1.3)	2.1 (1.1)
R_{merge} (%)[b]	2.1 (8.2)	2.0 (11.3)	2.2 (25.1)	4.2 (29.4)	3.1 (23.5)	3.3 (17.6)	2.2 (13.7)	2.1 (8.2)	4.3 (24.3)
$\langle I/\sigma(I)\rangle$[b]	28.1 (11.2)	24.0 (8.9)	23.1 (5.5)	14.2 (3.9)	18.7 (4.2)	17.2 (6.3)	23.5 (6.9)	25.4 (10.9)	14.3 (3.9)
Aniso-ADPs	Yes	Yes	Yes	No	Yes	Yes	Yes	No	No
Hydrogens	Yes	Yes	Yes	No	No	No	Yes	No	No
R/R_{free} (%)	11.9/13.3	13.2/15.5	13.6/15.3	18.0/25.2	12.6/16.1	16.3/20.8	14.0/15.9	18.5/25.0	17.1/24.0
$\langle B\rangle$ (Å^2)	10.4	15.11	14.0	33.2	20.1	17.1	15.5	23.1	31.5
Ramachandran core (%)	93.4	94.0	93.4	90.8	93.4	91.6	92.5	89.9	91.2
Ramachandran allowed (%)	6.1	5.7	6.1	8.8	6.1	7.5	7.0	9.6	8.3

All crystals belonged to the space group $P2_1$. Data were collected at 100° K. Reflections for R_{free} were randomly selected 5% of each dataset.
[a]These data are not discussed in the text, for completeness they are listed here and in the PDB.
[b]Value in parentheses describe the highest resolution shell

TABLE II. 3,5-Pyrazolediamine Inhibitors of *Ec*MAP

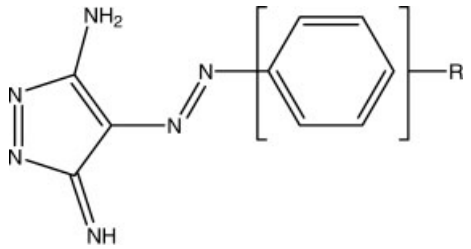

Compound	R	IC_{50} (μM)	Crystal structure
3	*m*-CF_3	0.25	2GG2
4	*o*-CF_3	0.25	2GG5
5	*m*-F	0.55	—
6	*m*-Cl, *o*-CH_3	0.55	—
7	*p*-F	0.58	2GG3
8	*p*-Cl	1.25	—
9	*p*-OCH_3	1.50	—
1, 2[a]	*m*-COOH	1.75	2GG7
10	*o*-OH, *m*-COOH	2.00	—
11	*p*-SO_2—NHNH—C(=NH)NH_2	20.0	—

[a]This compound initially was thought to be (**1**) but was actually (**2**). The IC_{50} value was obtained using (**2**) purchased from a different supplier.

TABLE III. Amino-Alcohol inhibitors of *Ec*MAP

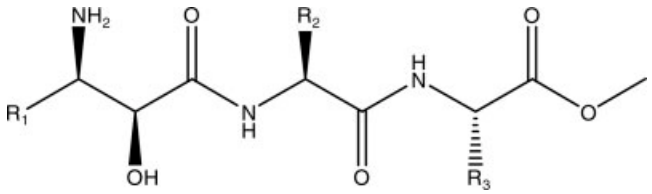

Compound	R_1	R_2	R_3	IC_{50} (μM)	Crystal Structure
12	*p*-CF_3—phenyl—	—CH_3	—	1.7	2GG0
13	*p*-*i*-Pr—phenyl—	—CH_3	*i*-butyl	3.5	2GG9
14	*n*-butyl—	—CH_2OH	*i*-butyl	12	2GGB
15	*p*-CH_3—phenyl—	—CH_3	*i*-butyl	25	2GG8

PDA Complexes

The pyrazole portion of these compounds is bound to the active-site cobalt ions via the electron pairs of the ring nitrogens [Fig. 2(a)]. The cobalt ion bound to His-171 is coordinated as a square pyramid composed of bonds of similar length (1.96–2.09 Å), whereas the coordination geometry of the other cobalt ion is a distorted trigonal bipyramid, which can also be perceived as a tetrahedron composed of shorter bond lengths (1.80–2.04 Å) with one additional ligand (Oδ2 of Asp-97) farther away (2.38 Å). Interestingly, the pyrazole ring is not coplanar with the line connecting the cobalt ions, instead the ring is offset by ~10°. One of the amino groups of the pyrazole moiety probably participates in a hydrogen bond with a ring nitrogen of His-178. The rest of the ligand is bound mostly through van der Waals contacts and p-stacking with several hydrophobic residues in the methionine-binding pocket of *Ec*MAP: His-79, Tyr-62, Tyr-65, Phe-177, Cys-70, Cys-59, His-63, and Trp-221 [Fig. 2(b)].

PDAs that were cocrystallized with *Ec*MAP are shown in Table II. Depending on the phenyl ring substituents, the portion of the ligand that is enclosed in the hydrophobic binding pocket adopts different orientations. Invariably upon PDAs binding the *Ec*MAP loop containing Trp-221 undergoes significant displacement. Compared to its position in the *Ec*MAP-Met complex, the loop moves ~1.5 Å outward, away from the catalytic site, to accommodate larger ligands (Fig. 3). At the same time, the loop containing Tyr-62 and His-63 moves closer to the ligand to optimize hydrophobic interactions in the binding pocket.

Amino$^-$ Alcohol Complexes

The AAs (Table III) bind to the enzyme in a manner that is very close to one previously described by Lowther

et al.[5] (Fig. 4). These fairly large compounds interact with *Ec*MAP active site as follows: in the metal-binding pocket the AAs coordinate the cobalt ions via both the alcohol and the primary amine, whereas in the methionine side-chain pocket the small molecules form hydrophobic contacts between the R_1 group (Table III) and the same residues that interact with the hydrophobic portion of PDAs as described earlier. This mode of binding requires precise spatial positioning of the interacting atoms, and therefore a stringent requirement for a specific AA diastereomer (it must be *R*, *S*), in a specific conformation (both the amine–hydroxyl and hydroxyl–carbonyl pairs must be *syn*clinal). It is very likely that this conformation does not represent a low local free energy minimum for most AA molecules, since the R_1 substituent experiences steric hindrance. Therefore, the binding of AA to *Ec*MAP is subject to free energy penalties—the enthalpic one, because of conformational rearrangement and the entropic one, because of elimination of multiple rotational degrees of freedom. To gain back potency, additional amino-acids (side chains R_2, R_3, Table III) are grafted on the AA core structure, these residues nonspecifically interact with the shallow channel on the surface of the *Ec*MAP enzyme. The discussion of the structure–activity relationship of AAs will be published elsewhere.

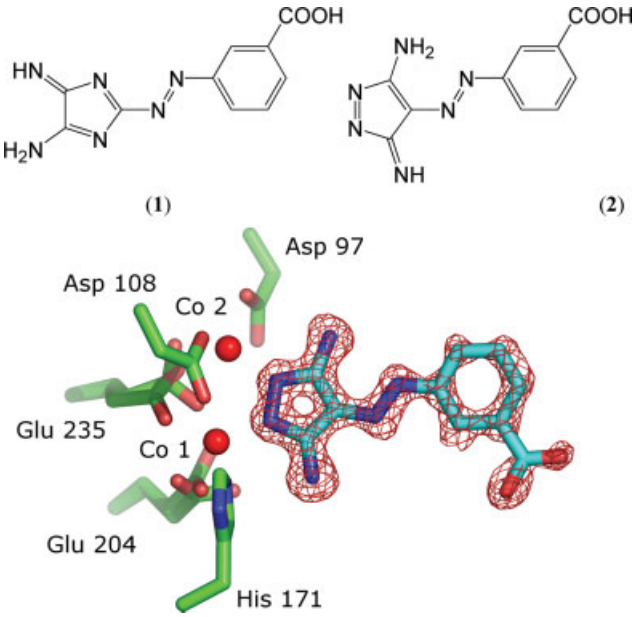

Fig. 1. The true identity of a PDA inhibitor. Difference electron density (red) in the EcMAP active site is contoured at four sigma, with the final inhibitor structure shown as blue stick model. Cobalt atoms and cobalt-chelating EcMAP residues are shown as spheres and sticks, respectively.

Methionine Complex

Our atomic-resolution structure of the *Ec*MAP in complex with methionine (PDBID: 2GGC) provides the most accurate measurements of MAP-methionine interactions to date. We were able to unambiguously place all the

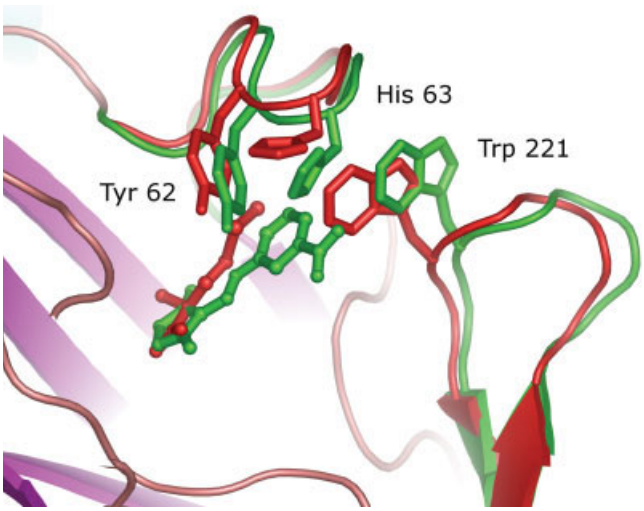

Fig. 3. Motion in the active site. Key residues that undergo significant movement upon displacement of methionine (red balls-and-sticks) in the active site by the PDA inhibitor (compound **2**) (green balls-and-sticks). Loops and residues are colored red and green for the methionine and the PDA complex respectively. The rest of the structure is shown as a cartoon.

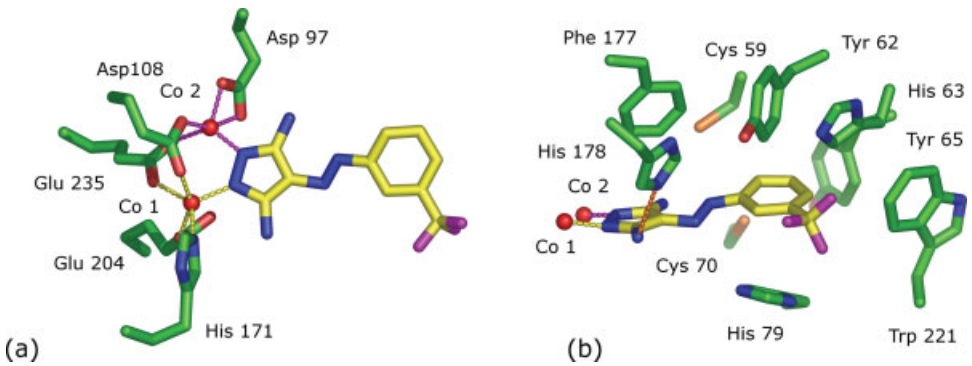

Fig. 2. Binding of a PDA (compound **3**) to EcMAP. (**a**) chelation of cobalt atoms (**b**) mostly hydrophobic interactions between the PDA and the enzyme active site residues. The inhibitor and protein residues are shown as stick models with carbon atoms colored green and yellow, respectively. Cobalt ions are shown as red spheres. Chelation spheres of Co_1 and Co_2 are shown as yellow and magenta dashes, respectively.

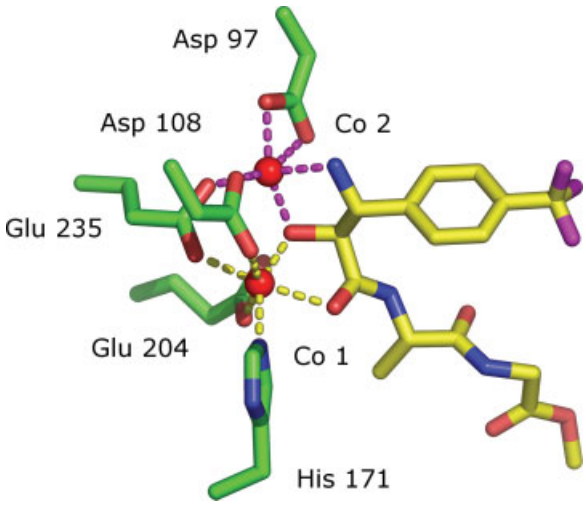

Fig. 4. Interaction of an AA inhibitor with the active site of EcMAP. The inhibitor and protein residues are shown as stick models with carbon atoms colored green and yellow, respectively. Cobalt ions are shown as red spheres. Chelation spheres of Co-1 and Co-2 are shown as yellow and magenta dashes, respectively. [Color figure can be viewed in the online issue, which is available at www.interscience.wiley.com.]

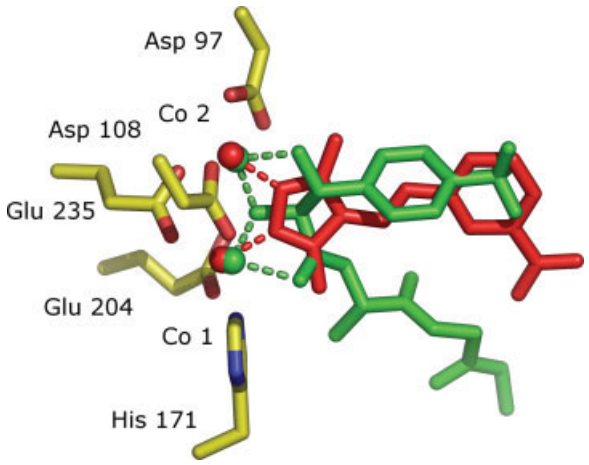

Fig. 5. Comparison of binding modes of PDA (red) versus AA (green). Cobalt ions and chelating interactions are shown as spheres and dashes, respectively. Active site residues are shown as stick models with carbon atoms colored yellow. [Color figure can be viewed in the online issue, which is available at www.interscience.wiley.com.]

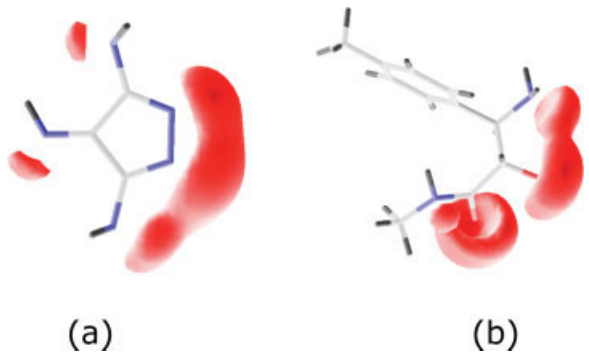

Fig. 6. Comparison of predicted electron density distribution in the vicinity of the chelating centers of PDA (**a**) and AA (**b**). Nitrogen, oxygen, carbon, and hydrogen atoms are colored blue, red, light, and dark grey, respectively. [Color figure can be viewed in the online issue, which is available at www.interscience.wiley.com.]

atoms of *Ec*MAP that were omitted from previous structures because of disorder (mostly missing or incomplete side chains). The binding of methionine to *Ec*MAP is relatively weak, as even at ~300-fold excess of the ligand only ~80% of the enzyme active sites are occupied. As was observed earlier,[5] methionine binds to the enzyme via electrostatic interactions of the charged portion of the amino acid with the cobalt ions and via the hydrophobic interactions of the side chain with the residues listed in the previous sections.

DISCUSSION

At the beginning of this project, we were faced with a puzzle: on the one hand, compound **1** was found to be a potent and selective inhibitor of *Ec*MAP, on the other hand its structural analogues found in our compound repository showed no inhibitory properties. This quandary was resolved by determination of the high-resolution X-ray crystal structure of the *Ec*MAP-**1** complex, which revealed that **1** was in fact compound **2**, whose structural relatives were later found to be potent inhibitors of *Ec*MAP.

Since the predicted interactions between *Ec*MAP and **1** were quite different from the experimentally determined *Ec*MAP-**2** interactions, we assume that the discovery of **2** as *Ec*MAP inhibitor was essentially serendipitous. The statistical probability of randomly encountering **2** or one of its analogues can be estimated from the following: there were 10 active structural analogues of **2** in the ~500,000 virtually screened compounds (using the 20 μM IC_{50} potency cutoff). In total, 130 virtual hits were tested in the enzyme assay; therefore the probability of purely random encounter was ~0.3%.

No other method would have provided us with both the knowledge of the true identity of the lead compound and the details of the interactions between the inhibitor and the enzyme at the same time. As a result, a synergy between several powerful screening and analysis methods has allowed us to discover a novel class of MAP inhibitors, the PDAs.

Atomic-resolution crystal structures of *Ec*MAP-inhibitor complexes allowed us to compare the mode of action of PDAs with that of the more traditional AAs derived from the natural product bestatin. The two modes of binding are shown in superimposition in Figure 5. Both the PDAs and the AAs inhibit *Ec*MAP through coordination with the binuclear metal center, augmented with and modulated by the hydrophobic interactions with the methionine-binding pocket of the enzyme. In the *Ec*MAP-AA complexes, the two electron pairs that are shared with the cobalt ions come from the same oxygen atom. We could not find any evidence of the bridging hydroxyl hydrogen atom in the 1.0 Å crystal structure of *Ec*MAP-AA complex. It is possible that the central oxygen of the

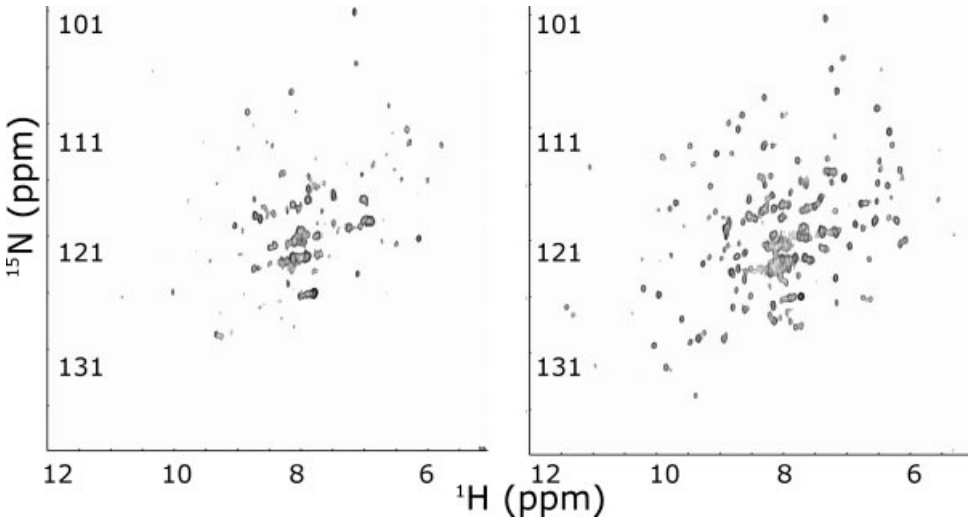

Fig. 7. Comparison of NMR spectra of the apo-EcMAP (left) and EcMAP in the presence of inhibitor (right).

AAs bears a negative charge similar to the hydroxyanion that has been suggested to bridge the cobalt ions of the unoccupied active site of the enzyme.[5] Additional ligand–metal interactions are in evidence in the *Ec*MAP-AA complexes, specifically the bond between Co-2 and the amine nitrogen and the bond between Co-1 and the carbonyl of the ligand. In the *Ec*MAP-PDA complexes, the electron pairs are abstracted by the cobalt ions from the two nitrogen atoms of the pyrazole ring. Unlike in the AA complexes, these two bonds are the only contacts between the ligand and the metal ions. Quantum–mechanical simulations of the PDA show twin areas of concentrated negative electrostatic potential located in front of the ring nitrogens [Fig. 6(a)]. Qualitatively, this potential is much more pronounced and more directional than that observed in the simulations of the AA [Fig. 6(b)]. Therefore, we suggest that the coordination between the PDA and the binuclear active center of the enzyme is significantly stronger than that between the active center and the AA. This hypothesis is supported by comparison of the AA and PDA modes of binding: to achieve single-digit micromolar IC_{50} values the AAs require at least 2–3 auxiliary amino-acid extensions that reside in the nonspecific peptide-binding pocket in addition to the interactions in the active site and the methionine pocket. In contrast, the PDAs have high nanomolar IC_{50} values while only binding to the active site and the methionine pocket. IC_{50} values as low as 250 n*M* were measured for compounds that were not optimized in any way, suggesting that with very modest effort the inhibitory potency of PDAs can be improved considerably.

Structure–Activity Relationship and Suggestions for Future Design

Discovery of the simple and potent PDA class of compounds opens a whole range of intriguing possibilities for improved inhibitor design. Analysis of the *Ec*MAP-PDA crystal structures suggests that within the scaffold described in this article the best potency can be achieved by introducing small hydrophobic substituents in the *ortho*- and *meta*-positions of the phenyl ring (e.g., compounds **3**, **4**, **5**, and **6**). Indeed, both the *o*-CF_3— and the *m*-CF_3— compounds have the lowest IC_{50} values within both the PDA and the AA series (Table III), with *m*-F— and *o*-CH3, *m*-Cl compounds taking the close second place. *Para*-substitution results in higher IC_{50} values (e.g., compounds **7**, **8**, and **9**), suggesting that the methionine side chain-mimetic group encounters progressively more resistance from Trp-221 as it extends deeper into the hydrophobic pocket of the enzyme. It is not entirely clear if the azo-link between the two portions of the PDA molecule can be altered, but it seems reasonable to expect that a suitable analogue could be devised, as long as the PDA heterocycle and the methionine sidechain-mimetic group are roughly coplanar.

Our studies of the PDA compounds indicate that it may be augmented or modified to offer new and intriguing options for inhibitor design. For example, the molecular crossbreeds of PDAs and AAs appear promising, especially in view of the fact that PDA-related heterocycles can be synthesized via standard chemistry routes, obviating the need for the more costly enantioselective synthesis or separation.

Human MAP 2 has been implicated in regulation of angiogenesis, and its overall fold and especially the structure of the catalytic site closely resemble those of bacterial aminopeptidase. The recently published papers[15,16] describe the crystal structures of complexes of human and *Staphylococcus* MAPs with heteroaromatic compounds that bind to the enzymes in a mode that is very similar to the interaction of PDAs with MAP. It is therefore very likely that PDAs and related scaffolds can be used to develop potent inhibitors of human MAP.

Insights into the Enzyme Mechanism

Recently, D'souza et al.[17] have proposed that bacterial MAPs are competent as single-metal enzymes. It is difficult to apply the available crystallographic data to the elucidation of the enzyme mechanism, since the truly native, unliganded structure of *Ec*MAP is not available—all the structures published to-date contain either an inhibitor molecule or a methionine in the active site. Nevertheless, we believe that some light may be shed on the enzymatic mechanism of *Ec*MAP by correlation of crystallographic evidence with that provided by NMR.

In the absence of inhibitor or substrate, ^{15}N-H *Ec*MAP NMR spectra are of poor quality (Fig. 7). This phenomenon can have multiple causes, for example, multiple interchanging conformational states of the protein, the presence of multiple metal-bound *Ec*MAP forms, aggregation, or partial unfolding of the protein. The catalytic activity of the enzyme is not compromised under the conditions of the NMR experiment, indicating that unfolding is not a likely possibility. There is also no evidence of aggregation in the dynamic light scattering experiments. Therefore we believe that poor NMR spectra observed for the enzyme in the absence of inhibitors are caused by rapid exchange of metal ions with solution as well as by rapid conformational changes of the protein for example, in the vicinity of the Trp-221 loop. Protein crystallization requires chemically as well as structurally homogenous sample, therefore it is not surprising that we failed to crystallize unliganded *Ec*MAP, which is structurally heterogeneous if the above logic is correct.

Addition of extra metal ions (up to 200 equivalents) results in only minor improvements in the appearance of the NMR spectra and does not allow for crystallization of the enzyme. Addition of inhibitors improves the spectra dramatically (Fig. 7) suggesting that multiple, rapidly interchanging forms of the enzyme become a dominant single state. Consequently, *Ec*MAP crystallization readily takes place in the presence of cobalt ions with either a large molar excess of methionine, or a small molar excess of a potent inhibitor.

In view of all the above, we speculate that in solution, in the absence of either inhibitor or substrate, *Ec*MAP undergoes both changes in conformation and rapid exchange of the weakly bound metal ion in the second site (Co-2 in our structures, Fig. 5). Upon binding of a substrate or an inhibitor, the second metal-binding site is augmented with at least one nitrogenous ligand that stabilizes the site in its metal ion-occupied state. With the second metal ion tightly bound, catalytic cleavage of the substrate takes place, whereupon the system dissociates, the products of the reaction and the second metal ion leave the active site, and the enzyme is ready to repeat the cycle. In the atomic resolution structure of *Ec*MAP-methionine complex, the occupancy of Co-2 and of the methionine is not full, both entities have the occupancy of 0.8, supporting the theory that the filled status of the second cobalt site is directly linked to the presence of the ligand. This hypothesis reconciles the binuclear *Ec*MAP active site model[18] with the alternative proposed by D'souza et al.[17]

In conclusion, we would like to stress the important role that structural biology can play in very early stages of drug discovery, using as an example the discovery of a new class of chemical agents that target MAPs. We hope that the PDA and related scaffolds may prove useful in the research and development of antibacterial drugs as well as antiangiogenesis agents.

ACKNOWLEDGMENTS

The authors thank Kenneth D. Greis and Thomas M. Burt (P & G Pharmaceuticals, Mason, OH) for determination of all mass spectra mentioned in this article.

REFERENCES

1. Vaughan MD, Sampson PB, Honek JF. Methionine in and out of proteins: targets for drug design. Curr Med Chem 2002;9:385–409.
2. Ingber D, Fujita T, Kishimoto S, Sudo K, Kanamaru T, Brem H, Folkman J. Synthetic analogues of fumagillin that inhibit angiogenesis and suppress tumour growth. Nature 1990;348:555–557.
3. Logothetis CJ, Wu KK, Finn LD, Daliani D, Figg W, Ghaddar H, Gutterman JU. Phase I trial of the angiogenesis inhibitor TNP-470 for progressive androgen-independent prostate cancer. Clin Cancer Res 2001;7:1198–1203.
4. Ohlstein EH, Ruffolo RR, Jr, Elliott JD. Drug discovery in the next millennium. Annu Rev Pharmacol Toxicol 2000;40:177–191.
5. Lowther WT, Orville AM, Madden DT, Lim S, Rich DH, Matthews BW. *Escherichia coli* methionine aminopeptidase: implications of crystallographic analyses of the native, mutant, and inhibited enzymes for the mechanism of catalysis. Biochemistry 1999;38:7678–7688.
6. Larrabee JA, Thamrong-nawasawat T, Mon SY. High-pressure liquid chromatographic method for the assay of methionine aminopeptidase activity: application to the study of enzymatic inactivation. Anal Biochem 1999;269:194–198.
7. Lowther WT, McMillen DA, Orville AM, Matthews BW. The antiangiogenic agent fumagillin covalently modifies a conserved active-site histidine in the *Escherichia coli* methionine aminopeptidase. Proc Natl Acad Sci USA 1998;95:12153–12157.
8. Navaza J. Implementation of molecular replacement in AMoRe. Acta Crystallogr D Biol Crystallogr 2001;57:1367–1372.
9. Jones TA, Zou JY, Cowan SW, Kjeldgaard. Improved methods for building protein models in electron density maps and the location of errors in these models. Acta Crystallogr A 1991;47:110–119.
10. Emsley P, Cowtan K. Coot: model-building tools for molecular graphics. Acta Crystallogr D Biol Crystallogr 2004;60:2126–2132.
11. Schneider TR, Sheldrick GM. Substructure solution with SHELXD. Acta Crystallogr D Biol Crystallogr 2002;58:1772–1779.
12. Murshudov GN, Vagin AA, Dodson EJ. Refinement of macromolecular structures by the maximum-likelihood method. Acta Crystallogr D Biol Crystallogr 1997;53:240–255.
13. Evdokimov AG, Kalb(Gilboa) AJ, Koetzle TF, Klooster WT, Martin JML. Structures of furanosides: density functional calculations and high-resolution X-ray and neutron diffraction crystal structures. J Phys Chem A 1999;103;744–753.
14. Frisch MJ, Trucks GW, Schlegel HB, Scuseria GE, Robb MA, Cheeseman JR, Zakrzewski VG, Montgomery JA, Stratmann RE, Burant JC, Dapprich S, Millam JM, Daniels AD, Kudin KN, Strain MC, Farkas O, Tomasi J, Barone V, Cossi M, Cammi R, Mennucci B, Pommelli C, Adamo C, Clifford S, Ochterski J, Petersson GA, Ayala PY, Cui Q, Morokuma K, Malick DK, Rabuck AD, Raghavachari K, Foresman JB, Cioslowski J, Ortiz JV, Stefanov BB, Liu G, Liashenko A, Piskorz P, Komaromi I, Gomperts R, Martin RL, Fox DJ, Keith T, Al-Laham MA, Peng CY, Nanayakkara A, Challacombe M, Gill PMW, Johnson BG, Chen W, Wong MW, Andres JL, Gonzales C, Head-Gordon M, Repogle ES, Pople JA. Gaussian 98. Pittsburg, PA: Guassian; 1998.

15. Kallander LS, Lu Q, Chen W, Tomaszek T, Yang G, Tew D, Meek TD, Hofmann GA, Schulz-Pritchard CK, Smith WW, Janson CA, Ryan MD, Zhang GF, Johanson KO, Kirkpatrick RB, Ho TF, Fisher PW, Mattern MR, Johnson RK, Hansbury MJ, Winkler JD, Ward KW, Veber DF, Thompson SK. 4-Aryl-1,2,3-triazole: a novel template for a reversible methionine aminopeptidase 2 inhibitor, optimized to inhibit angiogenesis in vivo. J Med Chem 2005;48:5644–5647.
16. Oefner C, Douangamath A, D'Arcy A, Hafeli S, Mareque D, Mac SA, Padilla J, Pierau S, Schulz H, Thormann M, Wadman S, Dale GE. The 1.15A crystal structure of the *Staphylococcus aureus* methionyl-aminopeptidase and complexes with triazole based inhibitors. J Mol Biol 2003;332:13–21.
17. D'souza VM, Swierczek SI, Cosper NJ, Meng L, Ruebush S, Copik AJ, Scott RA, Holz RC. Kinetic and structural characterization of manganese(II)-loaded methionyl aminopeptidases. Biochemistry 2002;41:13096–13105.
18. Lowther WT, Zhang Y, Sampson PB, Honek JF, Matthews BW. Insights into the mechanism of *Escherichia coli* methionine aminopeptidase from the structural analysis of reaction products and phosphorus-based transition-state analogues. Biochemistry 1999;38:14810–14819.